HAL
open science

Analysis of primal and dual variables in structural shape control by piezoelectric patches using solid-shell finite elements

Fessal Kpeky, Farid Abed-Meraim, El Mostafa Daya

To cite this version:

Fessal Kpeky, Farid Abed-Meraim, El Mostafa Daya. Analysis of primal and dual variables in structural shape control by piezoelectric patches using solid-shell finite elements. 8th ECCOMAS Thematic Conference on Smart Structures and Materials, Jun 2017, Madrid, Spain. pp.188-199. hal-01778396

HAL Id: hal-01778396

https://hal.science/hal-01778396v1

Submitted on 25 Apr 2018

HAL is a multi-disciplinary open access archive for the deposit and dissemination of scientific research documents, whether they are published or not. The documents may come from teaching and research institutions in France or abroad, or from public or private research centers.

L'archive ouverte pluridisciplinaire **HAL**, est destinée au dépôt et à la diffusion de documents scientifiques de niveau recherche, publiés ou non, émanant des établissements d'enseignement et de recherche français ou étrangers, des laboratoires publics ou privés.

VIII ECCOMAS Thematic Conference on Smart Structures and Materials
SMART 2017
A. Güemes, A. Benjeddou , J. Rodellar and Jinsong Leng (Eds)

ANALYSIS OF PRIMAL AND DUAL VARIABLES IN STRUCTURAL SHAPE CONTROL BY PIEZOELECTRIC PATCHES USING SOLID–SHELL FINITE ELEMENTS

F. KPEKY[*,‡], F. ABED-MERAIM[†,‡] AND E.M. DAYA[*,‡]

[*] Laboratoire d'Étude des Microstructures et de Mécanique des Matériaux (LEM3)
Université de Lorraine
Ile du Saulcy, 57045 Metz, France
e-mail: fessal.kpeky@univ-lorraine.fr, el-mostafa.daya@univ-lorraine.fr / www.lem3.fr

[†] Laboratoire d'Étude des Microstructures et de Mécanique des Matériaux (LEM3)
Arts et Métiers ParisTech
4 rue Augustin Fresnel, 57078 Metz, France
e-mail: farid.abed-meraim@ensam.eu / www.lem3.fr

[‡] Laboratory of Excellence on Design of Alloy Metals for low-mAss Structures (DAMAS)

Key words: Piezoelectric effect, Smart Structures, Finite elements, Solid–shell, Shape control.

Abstract. This paper presents an assessment of the performances of new piezoelectric solid–shell finite elements. Compared to conventional solid and shell elements, the solid–shell concept reveals to be very attractive, due to a number of well-established advantages and computational capabilities. This paper focuses on two element formulations, denoted SHB15E and SHB20E, which represent a quadratic prismatic solid–shell element and its hexahedral counterpart, respectively. The current analysis consists in an evaluation of primal and dual variables during the process of shape control of structures. The interest in this solid–shell approach is shown through a set of selective and representative plate and shell benchmark problems. The results obtained by the proposed formulations are compared with those given by state-of-the-art piezoelectric elements available in ABAQUS.

1 INTRODUCTION

Smart materials and structures are nowadays increasingly used in several areas of engineering. They can be found in automotive, aeronautics, aerospace, etc., where they are used for shape and vibration control [1-3], or in auscultation of civil infrastructures. They also have medical applications, such as pacemakers, civil engineering usage, where they serve to monitor the state of health of civil infrastructures [4-6], among many other fields. Piezoelectric materials, which represent a particular class of smart materials, have the ability

to generate an electrical potential when subjected to mechanical loading. They also have the ability to deform under application of electrical potential. These properties provide them interest in several engineering domains, where they are generally used as very thin transducers, or as sensors and actuators.

The prediction of the behavior of such materials therefore becomes important for their proper implementation. One of the least costly ways to do this is via numerical modeling, and most commonly through the finite element method. Since the early works of Allik and Hughes [7], several tools have been proposed in the literature to model piezoelectric structures. A large variety of 2D and 3D piezoelectric finite elements have actually been developed [8-10]. Examples of these are the Classical Laminate Plate Theory (CLPT) models, the Carrera Unified Formulation (CUF) models [11], among many others. Despite the availability of all of these models in the literature, worth noting is the lack of finite elements capable of low-cost modeling of structures combining thin and thick layers. Although, recently, authors such as Kulikov and Plotnikova [12, 13], as well as Nestorović et al. [14, 15], are stepping up to the proposal of solid–shell FE, the only alternative in commercial software packages like ABAQUS still remains the use of solid elements with refined meshes. To overcome these limitations, we have developed a family of piezoelectric finite elements using the solid–shell technology based on the works of Abed-Meraim et al. [16, 17]. These recently developed FE consist of hexahedral and prismatic solid–shell elements, using an in-plane reduced-integration scheme and a special direction designated as the “thickness”.

The main objective of this work is to assess the performance of the proposed elements through the calculation of primal and dual variables. To this end, the paper is organized as follows. Section 2 presents the coupled electromechanical constitutive equations as well as the discretized problem to be solved by the finite element method. Section 3 briefly outlines the formulation of the piezoelectric solid–shell elements. A set of selective and representative benchmark tests are conducted in Section 4, in order to assess the performance of the proposed piezoelectric solid–shell elements, for validation purposes. This paper is closed by Section 5, which summarizes the main contributions along with some concluding remarks.

2 CONSTITUTIVE EQUATIONS AND DISCRETIZATION OF THE PROBLEM

2.1 Electromechanical constitutive equations

Piezoelectric materials have the capability of generating electricity when subjected to mechanical loading (sensors). Conversely, they also have the ability to deform under electrical charging (actuators). These properties are described by the following coupled electromechanical equations:

$$\begin{cases} \boldsymbol{\sigma} = \mathbf{C} \cdot \boldsymbol{\varepsilon} - \mathbf{e}^T \cdot \boldsymbol{E} \\ \boldsymbol{D} = \mathbf{e} \cdot \boldsymbol{\varepsilon} + \boldsymbol{\kappa} \cdot \boldsymbol{E} \end{cases} \tag{1}$$

where $\boldsymbol{\sigma}$ and $\boldsymbol{\varepsilon}$ represent, respectively, the vector form of the stress and strain tensors; $\boldsymbol{D}$ and $\boldsymbol{E}$ denote the electric displacement and electric field vector, respectively; while $\mathbf{C}$, $\mathbf{e}$ and $\boldsymbol{\kappa}$ stand for the elastic, piezoelectric and dielectric permittivity matrix, respectively.

The discretized forms $\{\boldsymbol{\varepsilon}\}$ and $\{\boldsymbol{E}\}$ for the strain tensor and the electric field vector are related, respectively, to the discretized displacement $\{\boldsymbol{u}\}$ and to the discretized electric potential $\{\boldsymbol{\phi}\}$, using the discrete gradient operators $\left[\mathbf{B}^{u}\right]$ and $\left[\mathbf{B}^{\phi}\right]$, as follows:

$$\begin{cases} \{\boldsymbol{\varepsilon}\} = \left[\mathbf{B}^{u}\right]\{\boldsymbol{u}\} \\ \{\boldsymbol{E}\} = -\left[\mathbf{B}^{\phi}\right]\{\boldsymbol{\phi}\} \end{cases} \tag{2}$$

In the current contribution, the discrete gradient operators $\left[\mathbf{B}^{u}\right]$ and $\left[\mathbf{B}^{\phi}\right]$ are obtained by finite element discretization for each of the proposed piezoelectric solid–shell formulations SHB15E and SHB20E, as will be shown in Section 3 (see [18, 19] for more details).

2.2 Discretized problem

The variational principle pertaining to piezoelectric materials, which provides the governing equations for the associated boundary value problem, is described by the Hamilton principle [7]. In this weak form of equations of motion, the Lagrangian and the virtual work are appropriately adapted to include the electrical contributions, in addition to the more classical mechanical fields

$$\begin{aligned} &-\int_V \rho\ddot{\boldsymbol{u}}\cdot\delta\boldsymbol{u}\,dv - \int_V \boldsymbol{\sigma}\cdot\delta\boldsymbol{\varepsilon}\,dv + \int_V \boldsymbol{f}_v\cdot\delta\boldsymbol{u}\,dv + \int_S \boldsymbol{f}_s\cdot\delta\boldsymbol{u}\,ds + \boldsymbol{f}_p\cdot\delta\boldsymbol{u} \\ &= -\int_V \boldsymbol{D}\cdot\delta\boldsymbol{E}\,dv + \int_V \boldsymbol{q}_v\cdot\delta\boldsymbol{\phi}\,dv + \int_S \boldsymbol{q}_s\cdot\delta\boldsymbol{\phi}\,ds + \boldsymbol{q}_p\cdot\delta\boldsymbol{\phi} \end{aligned} \tag{3}$$

where ρ is the material density; $\boldsymbol{q}_v$, $\boldsymbol{q}_s$ and $\boldsymbol{q}_p$ denote volume, surface and point charge, respectively; while $\boldsymbol{f}_v$, $\boldsymbol{f}_s$ and $\boldsymbol{f}_p$ represent volume, surface and point force, respectively.

The finite element discretization of the boundary value problem governed by Eq. (3) generally leads to the following system of discretized equations:

$$\begin{cases} \left[\mathbf{M}^{uu}\right]\{\ddot{\boldsymbol{U}}\} + \left[\mathbf{K}^{uu}\right]\{\boldsymbol{U}\} + \left[\mathbf{K}^{u\phi}\right]\{\boldsymbol{\phi}\} = \{\boldsymbol{F}\} \\ \left[\mathbf{K}^{\phi u}\right]\{\boldsymbol{U}\} + \left[\mathbf{K}^{\phi\phi}\right]\{\boldsymbol{\phi}\} = \{\boldsymbol{Q}\} \end{cases} \tag{4}$$

where all matrices and vectors involved in Eq. (4) are explicitly defined in Table 1.

Table 1: Explicit forms for the vectors and matrices resulting from electromechanical coupling

$\left[\mathbf{M}^{uu}\right] = \int_V \left[\boldsymbol{N}^u\right]^T \rho \left[\boldsymbol{N}^u\right] dv$	Mass matrix
$\left[\mathbf{K}^{uu}\right] = \int_V \left[\mathbf{B}^u\right]^T \left[\mathbf{C}\right] \left[\mathbf{B}^u\right] dv$	Stiffness matrix
$\left[\mathbf{K}^{\phi\phi}\right] = -\int_V \left[\mathbf{B}^\phi\right]^T \left[\boldsymbol{\kappa}\right] \left[\mathbf{B}^\phi\right] dv$	Dielectric matrix
$\left[\mathbf{K}^{u\phi}\right] = \int_V \left[\mathbf{B}^u\right]^T \left[\mathbf{e}\right]^T \left[\mathbf{B}^\phi\right] dv;\ \left[\mathbf{K}^{\phi u}\right] = \left[\mathbf{K}^{u\phi}\right]^T$	Piezoelectric coupling matrix
$\{\boldsymbol{F}\} = \int_V \left[\boldsymbol{N}^u\right]^T \{\boldsymbol{f}_v\} dv + \int_S \left[\boldsymbol{N}^u\right]^T \{\boldsymbol{f}_s\} ds + \boldsymbol{f}_p$	Force vector
$\{\boldsymbol{Q}\} = -\int_V \left[\boldsymbol{N}^\phi\right]^T \{\boldsymbol{q}_v\} dv - \int_S \left[\boldsymbol{N}^\phi\right]^T \{\boldsymbol{q}_s\} ds - \boldsymbol{q}_p$	Electrical charge vector

3 PIEZOELECTRIC SOLID–SHELL FINITE ELEMENT FORMULATIONS

The proposed quadratic piezoelectric solid–shell finite elements SHB15E and SHB20E are extensions of the quadratic prismatic and hexahedral solid–shell elements SHB15 and SHB20, which were developed in [16], based on purely mechanical modeling. The starting point for these piezoelectric extensions is the addition of one piezoelectric degree of freedom to each node of their mechanical finite element counterparts. The outline of these formulations is given in the following sections.

3.1 Kinematics and interpolation

The piezoelectric solid–shell elements SHB15E and SHB20E denote a fifteen-node prismatic element and a twenty-node one, respectively. These elements have at each of their nodes three displacement degrees of freedom as well as one electric degree of freedom. Similar to their mechanical counterparts SHB15 and SHB20, a special direction is chosen, designated as the "*thickness*", normal to the mean plane of these elements. Also, an in-plane reduced-integration rule is adopted, with $3 \times n_{\text{int}}$ integration points for the SHB15E element and $4 \times n_{\text{int}}$ for the SHB20E (see, e.g., Fig. 1, in the particular case of $n_{\text{int}} = 5$).

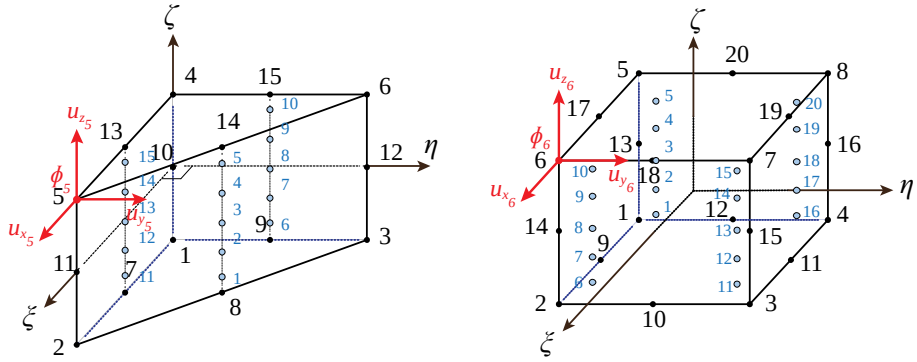

Figure 1: Schematic representation for the reference geometry of the SHB15E and SHB20E elements as well as for the location of their integration points in the case when the number of through-thickness integration points is $n_{\text{int}} = 5$

For the SHB15E and SHB20E elements, the spatial coordinates x_i are related to the nodal coordinates x_{iI} using quadratic shape functions, as follows:

$$x_i = x_{iI} N_I(\xi, \eta, \zeta) \tag{5}$$

where i represents the spatial directions and ranges from 1 to 3; while I stands for the node number, which ranges from 1 to 15, for the SHB15E element, and from 1 to 20 for the SHB20E. Likewise, the displacement field u_i and potential field ϕ are related to the nodal displacements u_{iI} and nodal potentials ϕ_I, respectively, using the shape functions

$$\begin{cases} u_i = u_{iI} N^u{}_I(\xi, \eta, \zeta) \\ \phi = \phi_I N^\phi{}_I(\xi, \eta, \zeta) \end{cases} \tag{6}$$

Note that in Eqs. (5) and (6) above, the convention of implied summation over the repeated index I has been adopted.

3.2 Discrete gradient operators

For both elements SHB15E and SHB20E, the corresponding discrete gradient operators $\left[\mathbf{B}^u\right]$ and $\left[\mathbf{B}^\phi\right]$ can be derived in the following compact form:

$$\mathbf{B}^u = \begin{bmatrix} \boldsymbol{b}_1^T + h_{\alpha,1}\boldsymbol{\gamma}_\alpha^T & \mathbf{0} & \mathbf{0} \\ \mathbf{0} & \boldsymbol{b}_2^T + h_{\alpha,2}\boldsymbol{\gamma}_\alpha^T & \mathbf{0} \\ \mathbf{0} & \mathbf{0} & \boldsymbol{b}_3^T + h_{\alpha,3}\boldsymbol{\gamma}_\alpha^T \\ \boldsymbol{b}_2^T + h_{\alpha,2}\boldsymbol{\gamma}_\alpha^T & \boldsymbol{b}_1^T + h_{\alpha,1}\boldsymbol{\gamma}_\alpha^T & \mathbf{0} \\ \boldsymbol{b}_3^T + h_{\alpha,3}\boldsymbol{\gamma}_\alpha^T & \mathbf{0} & \boldsymbol{b}_1^T + h_{\alpha,1}\boldsymbol{\gamma}_\alpha^T \\ \mathbf{0} & \boldsymbol{b}_3^T + h_{\alpha,3}\boldsymbol{\gamma}_\alpha^T & \boldsymbol{b}_2^T + h_{\alpha,2}\boldsymbol{\gamma}_\alpha^T \end{bmatrix} \quad ; \quad \mathbf{B}^\phi = \begin{bmatrix} \boldsymbol{b}_1^T + h_{\alpha,1}\boldsymbol{\gamma}_\alpha^T \\ \boldsymbol{b}_2^T + h_{\alpha,2}\boldsymbol{\gamma}_\alpha^T \\ \boldsymbol{b}_3^T + h_{\alpha,3}\boldsymbol{\gamma}_\alpha^T \end{bmatrix} \tag{7}$$

where the expressions of $\boldsymbol{b}_j^T$, $h_{\alpha,j}$ and $\boldsymbol{\gamma}_\alpha^T$ can be found in reference [16], along with additional details on their derivation. Note again that, in Eq. (7) and in what follows, the convention of implied summation over the repeated index α is adopted, with α ranging from 1 to 11, for the SHB15E element, and from 1 to 16 for the SHB20E.

Similar to the purely mechanics-based solid–shell elements SHB15 and SHB20 (see, e.g., [16]), the benchmark tests performed with the piezoelectric solid–shell counterparts SHB15E and SHB20E did not reveal any particular locking and, accordingly, no specific enhanced assumed strain techniques have been applied to these quadratic solid–shell elements.

4 NUMERICAL TESTS AND DISCUSSIONS

In this Section, a set of representative plate and shell benchmark tests is conducted to evaluate the performance of the proposed piezoelectric solid–shell finite elements.

4.1 Shape control of square plate with piezoelectric patch models

One important advantage taken from the piezoelectric behavior is in the application to the shape control of structures. In order to show the interest of solid–shell finite elements in this type of modeling, we consider a square aluminum plate of 200×200 mm^2 with a thickness of 8 mm. This plate is covered on both sides with a pair of localized PZT-5H patches, as shown in Fig. 2. Each patch has dimensions of 80×80 mm^2 with a thickness of 1 mm. The material parameters are reported in Table 2. With regard to loading conditions, the plate is subjected to a uniformly distributed load of 100 N.m^{-2} over its entire surface. A constant voltage is then supplied incrementally to the PZT-5H actuators, which are polarized in opposite directions, until the plate is flattened. Fig. 3 shows the magnitude of deflection of the composite plate under different applied input voltages. The results provided by the solid–shell elements SHB15E and SHB20E are reported in Tables 3 and 4, where they are compared with the results given by the ABAQUS solid elements C3D15E and C3D20E. On the whole, it appears that fewer overall degrees of freedom (dof) are required for the proposed piezoelectric solid–shell elements to achieve convergence, as compared to ABAQUS elements.

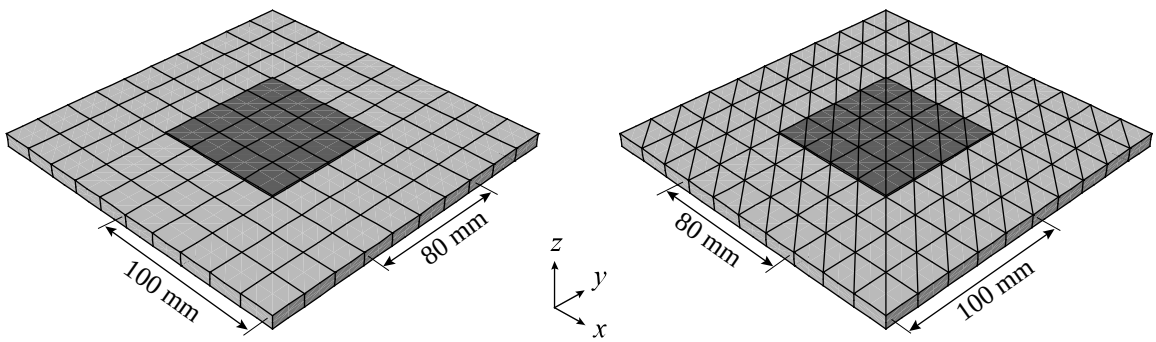

Figure 2: Schematic representation of the square plate with piezoelectric patches meshed with SHB15E and SHB20E elements

Table 2: Material properties used for all simulations

PZT-5H	$C_{11} = C_{22} = 127.2$ GPa ; $C_{33} = 117.4$ GPa $C_{12} = 80.21$ GPa ; $C_{13} = C_{23} = 84.67$ GPa $C_{44} = C_{55} = C_{66} = 22.99$ GPa $e_{15} = e_{24} = 17.03$ C/m^2 $e_{31} = e_{32} = -6.62$ C/m^2 ; $e_{33} = 23.24$ C/m^2 $\kappa_{11} = \kappa_{22} = 1.509 \times 10^{-8}$ F/m ; $\kappa_{33} = 1.269 \times 10^{-8}$ F/m
Aluminum	E = 70.3 GPa ; $\nu = 0.345$

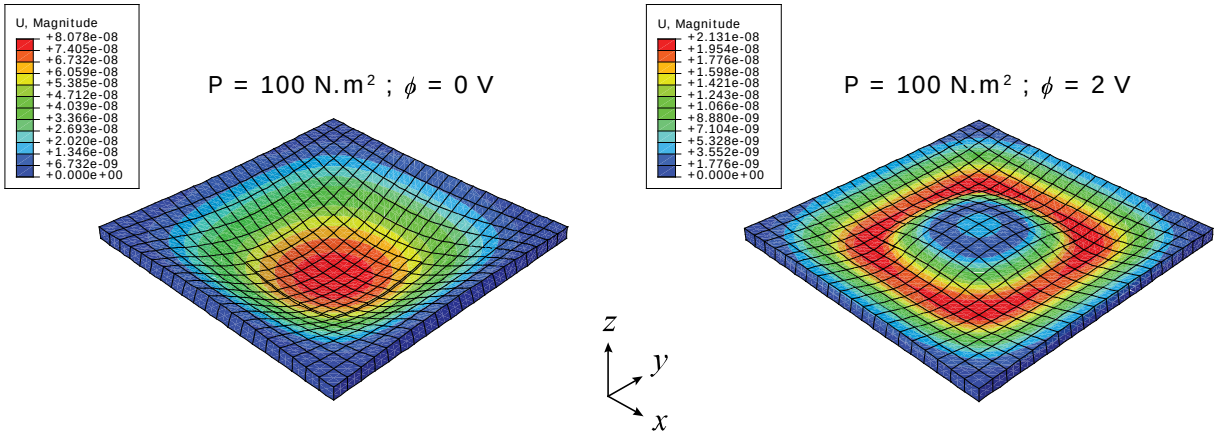

Figure 3: Shape of the plate for two different applied voltages

Table 3: Primal and dual variables for the plate shape control test (P=100N.m^2; ϕ=0V)

	C3D15E (20×20×3)×2	**SHB15E** (10×10×3)×2	**C3D20E** (20×20×3)	**SHB20E** (10×10×3)
Primal variables				
U_z^{max} (m)	8.111×10^{-8}	8.047×10^{-8}	8.078×10^{-8}	8.183×10^{-8}
Dual variables				
ε_{zz}^{min}	-9.965×10^{-8}	-1.100×10^{-7}	-9.920×10^{-8}	-1.001×10^{-7}
ε_{zz}^{max}	1.556×10^{-7}	1.780×10^{-7}	1.546×10^{-7}	1.832×10^{-7}
σ_{xx}^{mn} (Pa)	-6.554×10^{3}	-6.133×10^{3}	-6.233×10^{3}	-6.752×10^{3}
σ_{xx}^{max} (Pa)	8.100×10^{3}	7.780×10^{3}	7.892×10^{3}	7.653×10^{3}
E_z^{min} (V.m^{-1})	-9.229×10^{1}	-9.323×10^{1}	-9.240×10^{1}	-9.297×10^{1}
E_z^{max} (V.m^{-1})	9.229×10^{1}	9.323×10^{1}	9.240×10^{1}	9.292×10^{2}
D_z^{min} (C.m^{-2})	-2.961×10^{-6}	-3.094×10^{-6}	-2.950×10^{-6}	-3.026×10^{-6}
D_z^{max} (C.m^{-2})	4.782×10^{-6}	4.713×10^{-6}	4.757×10^{-6}	4.782×10^{-6}

Table 4: Primal and dual variables for the plate shape control test (P=100N.m^2; ϕ=2V)

	C3D15E (20×20×3)×2	**SHB15E** (10×10×3)×2	**C3D20E** (20×20×3)	**SHB20E** (10×10×3)
Primal variables				
U_z^{max} (m)	2.182×10^{-8}	2.220×10^{-8}	2.130×10^{-8}	2.177×10^{-8}
Dual variables				
ε_{zz}^{min}	-8.962×10^{-7}	-8.987×10^{-7}	-8.749×10^{-7}	-8.954×10^{-7}
ε_{zz}^{max}	9.076×10^{-7}	9.292×10^{-7}	8.971×10^{-7}	8.889×10^{-7}
σ_{xx}^{mn} (Pa)	-7.381×10^{4}	-7.488×10^{4}	-6.905×10^{4}	-7.325×10^{-4}
σ_{xx}^{max} (Pa)	7.039×10^{4}	6.838×10^{4}	6.827×10^{4}	7.005×10^{-4}
E_z^{min} (V.m^{-1})	-2.315×10^{3}	-2.259×10^{3}	-2.289×10^{3}	-2.122×10^{3}
E_z^{max} (V.m^{-1})	2.284×10^{3}	2.274×10^{3}	2.277×10^{3}	2.181×10^{3}
D_z^{min} (C.m^{-2})	-4.656×10^{-5}	-4.576×10^{-5}	-4.220×10^{-5}	-4.397×10^{-5}
D_z^{max} (C.m^{-2})	4.712×10^{-5}	4.677×10^{-5}	4.206×10^{-5}	4.242×10^{-5}

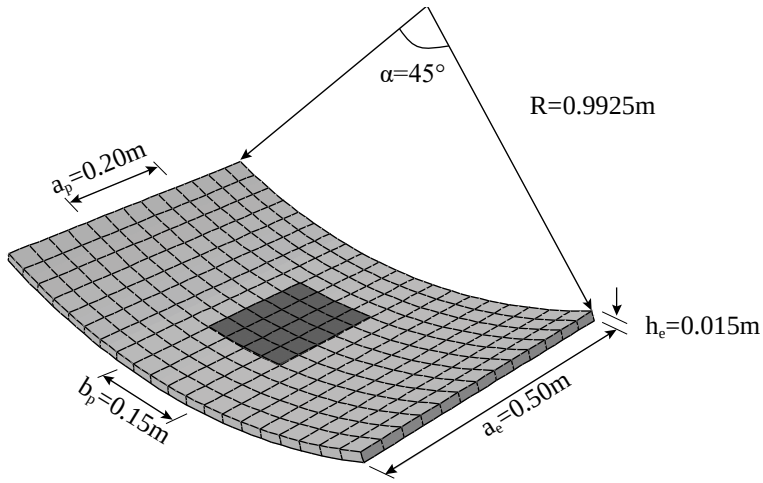

Figure 4: Schematic representation of the curved shell with piezoelectric patch meshed with C3D20E

4.2 Curved shell with piezoelectric patches

This benchmark test is inspired by the tests performed by Koconis et al. [20, 21], who proposed models for the shape control of shell structures. Here, we consider a simply supported curved shell, on top of which is bonded a localized PZT-5H patch with a thickness of 1 mm, as shown in Fig. 4. All other geometric parameters are also indicated in this figure. A constant voltage $\phi = 10$ V is then applied to the PZT-5H actuator, which is polarized in the thickness. Similar to the preview test, the results provided by the solid–shell elements SHB15E and SHB20E are compared with those given by the ABAQUS solid elements C3D15E and C3D20E. A convergence study is conducted on different variable fields in order to identify the minimum number of degrees of freedom required to achieve convergence for all variables. In Figs. 5–7, are presented the convergence curves and field maps for the tip displacement, the strain, and the electric flux, respectively. From this convergence analysis, it appears that fewer degrees of freedom are required for the proposed solid–shell finite elements to achieve convergence, as compared to ABAQUS elements. More specifically, less dof are required for the computation of primal variables, as compared to the computation of dual variables. Indeed, about 10,000 dof reveal sufficient to evaluate the displacement with an error margin smaller than 5%, whereas 10 times more dof are needed to obtain deformations and electric flux within the same margin of error.

This test also allows us to emphasize some additional advantages of the solid–shell concept, compared to standard finite elements, especially in situations where the geometry is curved.

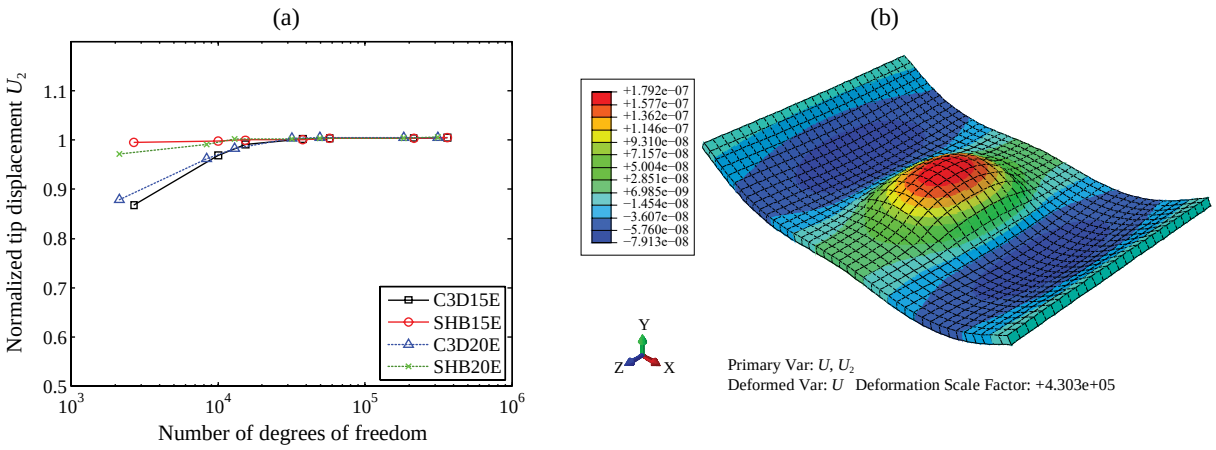

Figure 5: (a) Convergence curves and (b) Field map of displacement U_2 for the actuated curved shell

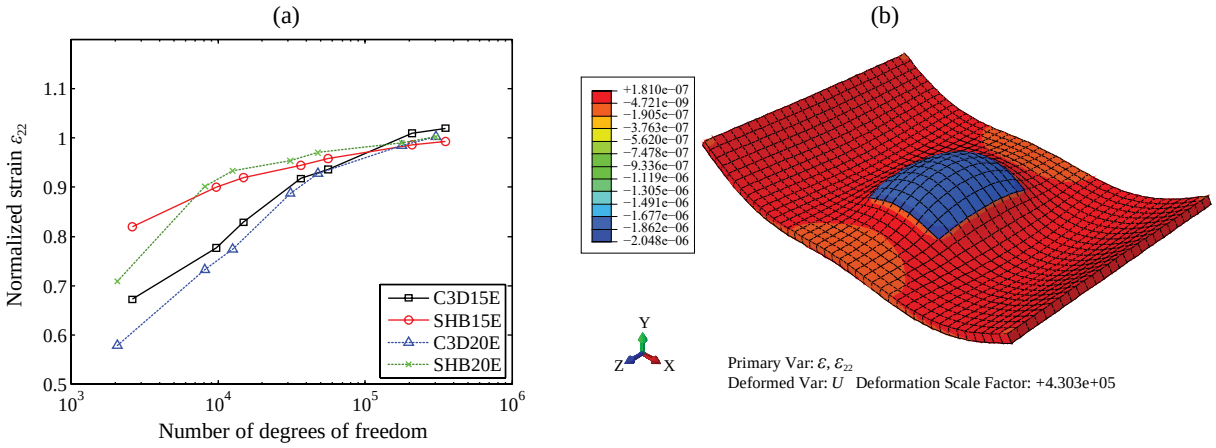

Figure 6: (a) Convergence curves and (b) Field map of strain ε_{22} for the actuated curved shell

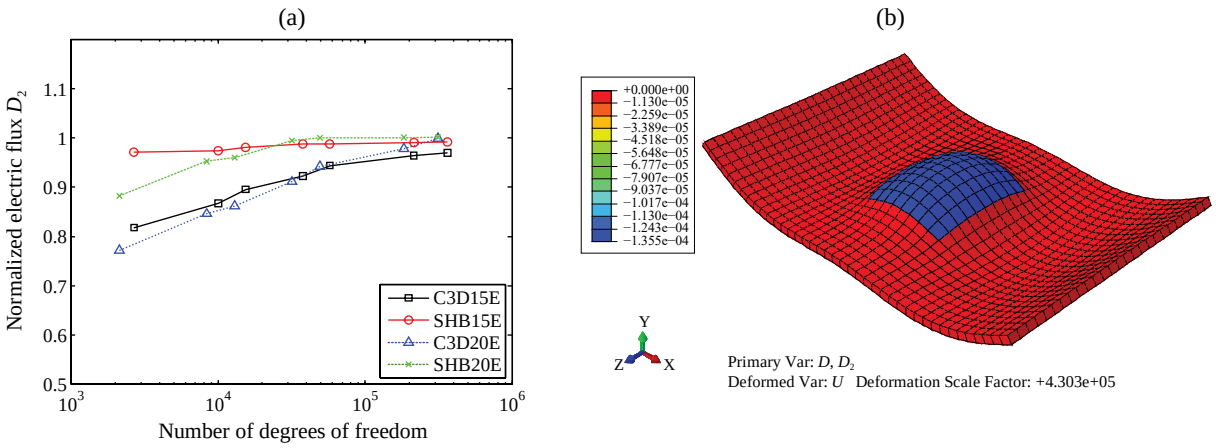

Figure 7: (a) Convergence curves and (b) Field map of electric flux D_2 for the actuated curved shell

5 CONCLUSIONS

In this paper, a performance assessment of recently proposed piezoelectric solid–shell finite elements has been presented. The analysis consists in an evaluation of primal and dual variables under electromechanical loading conditions. These investigations are conducted in the context of shape control of structures. A set of selective and representative benchmark tests has been performed on plate and shell structures, on which piezoelectric patches are bonded. The obtained simulation results have been compared to their counterparts given by state-of-the-art finite elements available in ABAQUS. In all of the benchmark tests investigated, the proposed quadratic solid–shell elements have shown better performance, as compared to their ABAQUS counterparts, while systematically necessitating much less degrees of freedom for similar accuracy. It has also been revealed that particular attention should be paid to the modeling of electromechanical coupling in order to improve the efficient computation of dual variables.

REFERENCES

[1] Belouettar, S., Azrar, L., Daya, E.M., Laptev, V. and Potier-Ferry, M. Active control of nonlinear vibration of sandwich piezoelectric beams: A simplified approach. *Computers and Structures* (2008) **86**:386-397.

[2] Nguyen, Q. and Tong, L. Voltage and evolutionary piezoelectric actuator design optimisation for static shape control of smart plate structures. *Materials & Design* (2007) **28**:387-399.

[3] Olsen, H.F. Electronic control of noise, vibration and reverberation. *Journal of the Acoustical Society of America* (1956) **28**:972-976.

[4] Duan, W.H., Wang, Q. and Quek, S.T. Applications of Piezoelectric Materials in Structural Health Monitoring and Repair: Selected Research Examples. *Materials* (2010) **3**:5169-5194.

[5] Park, G., Cudney, H. and Inman, D. Impedance-based health monitoring of civil structural components. *Journal of Infrastructure Systems* (2000) **6**:153-160.

[6] An, Y.K., Kim, M.K. and Sohn, H. Piezoelectric transducers for assessing and monitoring civil infrastructures. *Sensor Technologies for Civil Infrastructures* (2014) **55**:86-120.

[7] Allik, H. and Hughes, T.J.R. Finite element method for piezoelectric vibration. *International Journal for Numerical Methods in Engineering* (1970) **2**:151-157.

[8] Mindlin, R.D. Forced Thickness-Shear and Flexural Vibrations of Piezoelectric Crystal Plates. *Journal of Applied Physics* (1952) **23**:83-88.

[9] Plagianakos, T.S. and Papadopoulos, E.G. Higher-order 2-D/3-D layerwise mechanics and finite elements for composite and sandwich composite plates with piezoelectric layers. *Aerospace Science and Technology* (2015) **40**:150-163.

[10] Shiyekar, S.M. and Kant, T. Higher order shear deformation effects on analysis of laminates with piezoelectric fibre reinforced composite actuators. *Composite Structures* (2011) **93**:3252-3261.
[11] Robaldo, A., Carrera, E. and Benjeddou, A. A unified formulation for finite element analysis of piezoelectric adaptive plates. *Computers & Structures* (2006) **84**:1494-1505.
[12] Kulikov, G.M. and Plotnikova, S.V. Geometrically exact four-node piezoelectric solid-shell element. *Mechanics of Advanced Materials and Structures* (2008) **15**:199-207.
[13] Kulikov, G.M. and Plotnikova, S.V. The Use of 9-Parameter Shell Theory for Development of Exact Geometry 12-Node Quadrilateral Piezoelectric Laminated Solid-Shell Elements. *Mechanics of Advanced Materials and Structures* (2014) **22**:490-502.
[14] Nestorović, T., Marinković, D., Chandrashekar, G., Marinković, Z. and Trajkov, M. Implementation of a user defined piezoelectric shell element for analysis of active structures. *Finite Elements in Analysis and Design* (2012) **52**:11-12.
[15] Nestorović, T., Marinković, D., Shabadi, S. and Trajkov, M. User defined finite element for modeling and analysis of active piezoelectric shell structures. *Meccanica* (2014) **49**:1763-1774.
[16] Abed-Meraim, F., Trinh, V.D. and Combescure, A. New quadratic solid–shell elements and their evaluation on linear benchmark problems. *Computing* (2013) **95**:373-394.
[17] Abed-Meraim, F. and Combescure, A. An improved assumed strain solid-shell element formulation with physical stabilization for geometric non-linear applications and elastic-plastic stability analysis. *International Journal for Numerical Methods in Engineering* (2009) **80**:1640-1686.
[18] Kpeky, F., Abed-Meraim, F., Boudaoud, H. and Daya, E.M. Linear and quadratic solid–shell finite elements SHB8PSE and SHB20E for the modeling of piezoelectric sandwich structures. *Mechanics of Advanced Materials and Structures* (2017) http://dx.doi.org/10.1080/15376494.15372017.11285466.
[19] Kpeky, F., Abed-Meraim, F. and Daya, E.M. New linear and quadratic piezoelectric solid-shell finite elements. *Applied Mathematics and Computation*, in press (2017).
[20] Koconis, D.B., Kollår, L.P. and Springer, G.S. Shape control of composite plates and shells with embedded actuators. II. Desired shape specified. *Journal of Composite Materials* (1994) **28**:262-285.
[21] Koconis, D.B., Kollår, L.P. and Springer, G.S. Shape control of composite plates and shells with embedded actuators. I. Voltages specified. *Journal of Composite Materials* (1994) **28**:415-458.